

1 **Diffusion of ionic tracers in the Callovo-Oxfordian clay-rock using**
2 **the Donnan equilibrium model and the electrical formation factor**

3
4 D. Jougnot (1, 2, 3), A. Revil (2, 3), and P. Leroy (4)

5
6 1. ANDRA, 1-7 rue Jean Monnet, 92298 Châtenay-Malabry, France

7 2. CNRS-UMR 5559-LGIT, Université de Savoie, Equipe volcan, 73376 Le-Bourget-du-Lac, France

8 3. Colorado School of Mines, Department of Geophysics, Golden, 80401, CO, USA

9 4. BRGM, 3 avenue C. Guillemin, BP 6009, 45061 Orléans, France

10 _____
11
12 **Corresponding author:**

13 Damien Jougnot

14 Colorado School of Mines, Dept of Geophysics

15 1500 Illinois street, Golden, CO, 80401.

16 djougnot@mines.edu

ABSTRACT

The transient diffusion of cationic and anionic tracers through clay-rocks is usually modeled with parameters like porosity, tortuosity (and/or constrictivity), sorption coefficients, and anionic exclusion. Recently, a new pore scale model has been developed by Revil and Linde (2006). This model is based on a volume-averaging approach of the Nernst-Planck equation. In this model, the influence of the electrical diffuse layer is accounted for by a generalized Donnan equilibrium model that is valid for a multicomponent electrolyte. This new model is able to reproduce a number of observations including the determination of the composition of the pore water of the Callovo-Oxfordian argillite, the determination of the osmotic efficiency of bentonite as a function of salinity, the osmotic pressure, and the streaming potential coupling coefficient of clay-rocks. This pore scale model is used here to model the transient diffusion of ionic tracers ($^{22}\text{Na}^+$, $^{36}\text{Cl}^-$, and $^{35}\text{SO}_4^{2-}$) through the Callovo-Oxfordian low-porosity argillite. Using experimental data from the literature, we show that all the parameters required to model the flux of ionic tracers (especially the mean electrical potential of the pore space and the formation factor) are in agreement with a previous evaluation of these parameters using totally independent rock properties including the osmotic pressure and HTO diffusion experiments. This confirms that the pore scale model of Revil and Linde (2006) is able to model a high number of transport phenomena into a unified framework.

1. INTRODUCTION

45

46 The diffusion of ions in charged porous media like clay materials has been studied by
47 a number of researchers for a variety of geoenvironmental applications including ground
48 water contamination from clay-lined landfills (Malusis and Shackelford, 2003) and the
49 spreading of contaminants from canisters containing nuclear wastes (Chatterji, 2004). The
50 possibility to use clay-rocks as a potential host for the long-term isolation of nuclear wastes
51 has recently driven new researches in this field. The French Nuclear Waste Agency (ANDRA)
52 is presently studying the long-term storage of high-level long-lived nuclear wastes in the
53 Callovo-Oxfordian (Cox) clay-rock formation in the East portion of the Paris basin (ANDRA,
54 2005). The Cox clay-rock is composed of clay-minerals (between 20 and 50 % in mass
55 fraction), silica, and carbonates. Because of the very low intrinsic permeability of this
56 formation (in the range 10^{-19} to 10^{-21} m², see Escoffier et al., 2000; Gasc-Barbier et al., 2004),
57 diffusion of ions is considered to be the major mechanism of the potential spread of ionic
58 species in the bentonite and in the clay-rock formation.

59 To understand the diffusion of ions in such a complex material, new experiments were
60 performed recently to evaluate the diffusion and the sorption of radio-isotopic elements
61 (Melkior et al. 2004, 2005, 2007; Bazer-Bachi et al. 2005, 2007 and references therein).
62 However, these authors used phenomenological models and empirical parameters to explain
63 why the diffusion coefficient of some sorbed cationic species (like Na⁺, K⁺, or Cs⁺) are higher
64 than diffusion coefficient of anions (e.g. chloride). Their approach does not take into account
65 explicitly the influence of the microstructure and electrochemical properties of the
66 mineral/water interface on the diffusivity of ions.

67 Recently, Appelo and Wersin (2007) used a generalized Donnan equilibrium model to
68 include the effect of the diffuse layer at the mineral/water interface of clay materials upon the
69 diffusivity of ionic species. However, their model does not consider the existence of the Stern

70 layer where most of the charged counterions are located (Leroy and Revil, 2004; Leroy et al.,
71 2007, 2008). Their macroscopic transport model is also not explicitly connected to the
72 microscopic phenomena at the mineral/water interface.

73 In this paper, we are interested to test the approach developed recently by Revil and
74 Linde (2006), Revil (2007), and Leroy et al. (2007). Revil and Linde (2006) and Revil (2007)
75 developed a unifying model of transport properties of water and ions in charged microporous
76 materials. This model is obtained by upscaling the local constitutive equations (Nernst-Planck
77 and Navier-Stokes equations) using a volume-averaging operator. Consequently, the
78 constitutive equations established some simple, and theoretically-based, relationships between
79 the measurable material properties, the key-microstructural parameters of the porous medium
80 (formation factor and intrinsic permeability), and to the electrochemical properties of the
81 double layer coating the clay particles. This model was recently extended to include the effect
82 of partial saturation upon electrokinetic properties (Linde et al., 2007; Revil et al., 2007) and
83 the diffusion of ions in a concentration field for partially saturated media (Revil and Jougnot,
84 2008). Leroy et al. (2007) have also modeled the composition of the pore water of the
85 Callovo-Oxfordian clay-rock using an extension of this model.

86 In the present paper, we adapt this modeling approach in order to study the diffusion of
87 radioactive tracers in a clay-rock. After a rapid review of the classical diffusion models used
88 in the literature to interpret such type of data, we will present the microscopic description and
89 underlying assumptions of our tracer diffusion model. This model will be tested against recent
90 experimental data using a variety of 3 radioactive tracers ($^{22}\text{Na}^+$, $^{36}\text{Cl}^-$, $^{35}\text{SO}_4^{2-}$) on different
91 samples of the Callovo-Oxfordian clay-rock in the porosity range 0.03-0.15. The model will
92 show also a consistency between the mean electrical potential existing in the pore space of the
93 clay-rock and the electrical potential needed to explain the osmotic pressure in the Cox
94 formation.

95

96

2. STATE OF THE ART

97

98

The diffusion of ions through a porous material is classically based on the Fick constitutive equation. The flux of the species i through a porous material, \mathbf{J}_i (in mol m⁻² s⁻¹) is

100

usually described by the first Fick's law,

101

$$\mathbf{J}_i = -D_i \nabla C_i, \quad (1)$$

102

where D_i is the effective diffusion coefficient in the medium (in m² s⁻¹) and C_i the

103

concentration of species i in the porous medium (in mol m⁻³). The concentrations, usually

104

expressed in mol L⁻¹, are expressed below in m⁻³ in the metric system. Several models have

105

been developed to express D_i in terms of the textural properties of the porous material (see

106

Bourg et al., 2003, Bourg, 2004 for some phenomenological models and Melkior et al., 2007

107

for a short review of the literature). It is notoriously known that porosity cannot be used alone

108

to determine the diffusion coefficient. Additional fitting parameters, such as tortuosity or

109

constrictivity, have been introduced to account for the fact that only a fraction of the porosity

110

is used by the migration of ions through the pore space or to account for the tortuous path of

111

the ions during their migration through the pore space. One of the most popular models to

112

account for tortuosity was developed by Van Brakel and Heertjes (1974). It yields,

113

$$D_i = \phi D_i^f \frac{\delta}{\tau^2}, \quad (2)$$

114

where D_i^f (in m² s⁻¹) is the self-diffusion coefficient of species i in the bulk pore water, ϕ is

115

the porosity, τ is the tortuosity of the bulk pore space, and δ is the constrictivity. Further in

116

this paper, we will propose to distinguish two components in the constrictivity parameter: an

117 geometrical constrictivity (δ_g) for the pore space topography and an electrostatic constrictivity
 118 (δ_{el}) for the electrostatic interactions between ions and charged mineral surfaces.

119 The continuity equation for the species i , in a porous medium, can be expressed by the
 120 second Fick's law:

$$121 \quad \phi \frac{\partial C_i}{\partial t} + (1 - \phi) \rho_g \frac{\partial C_i^S}{\partial t} = -\nabla \cdot \mathbf{J}_i, \quad (3)$$

122 with C_i^S the concentration of ions i that are sorbed onto the mineral surface (in mol kg⁻¹), ρ_g
 123 the grain density (in kg m⁻³), and t the time (in s). The second term of Eq. (3) corresponds to a
 124 source / sink term that is associated with the interactions of the solution with the surface of the
 125 minerals. Sorption of solutes in a porous medium can be modeled by simple isotherms (see
 126 Limousin et al., 2007 for a recent review) or models accounting for electrical double or triple
 127 layer theory (Leroy and Revil, 2004; Leroy et al., 2007). Assuming that the ratio between the
 128 sorbed concentration and solution concentration is constant with time, it is customary to
 129 introduce a distribution or partitioning coefficient defined by $K_d^i = C_i^S / C_i$ (in m³ kg⁻¹) (e.g.,
 130 Limousin et al., 2007). Using this definition, Eq (3) can be written as follow:

$$131 \quad \left[\phi + (1 - \phi) \rho_g K_d^i \right] \frac{\partial C_i}{\partial t} = -\nabla \cdot \mathbf{J}_i. \quad (4)$$

132 Introducing the effective sorption and the first Fick's law in Eq. (4) yields the classical
 133 diffusion equation in this equation,

$$134 \quad \frac{\partial C_i}{\partial t} = \nabla \cdot (\eta_i \nabla C_i) \quad (5)$$

135 where η_i , the apparent diffusivity of ion i , is defined by,

$$136 \quad \eta_i = \frac{D_i}{\left[\phi + (1 - \phi) \rho_g K_d^i \right]}. \quad (6)$$

137 Note that in this paper, we use the expression “diffusion coefficient” to describe the material
 138 properties arising in first Fick law (which is the constitutive equation) and the term

139 “diffusivity” to describe the material properties arising in the diffusion equation obtained by
 140 combining the first and second Fick’s law. If sorption can be neglected for a given tracer, the
 141 diffusivity of this tracer is equal to the ratio between the effective diffusion coefficient and the
 142 porosity $\eta_i = D_i/\phi$ (Revil and Leroy, 2004; Revil et al., 2005).

143 The previous model is however too simplistic. It does not account for the
 144 concentrations of the ionic species in the micropores because of the existence of the electrical
 145 diffuse layer. To account for this effect, Muurinen et al. (1988) proposed the introduction of
 146 an effective porosity ϕ_{eff} in the mass conservation equation. This yields:

$$147 \quad \phi_{eff_i} \frac{\partial C_i}{\partial t} = \nabla \cdot \left(\frac{\phi_{eff_i} D_i^f}{\tau^2} \nabla C_i \right). \quad (7)$$

148 For anions, this effective porosity can also be modeled by using a negative value of the
 149 distribution coefficient. This very popular approach is however phenomenological in nature
 150 and ϕ_{eff} is a fitting parameter that takes different values for different ions.

151 Bourg (2004) proposed a diffusion model in bentonite. This model divides the medium
 152 in three parallel pore networks: a macroporous one and two microporous (a two-layer and a
 153 three-layer water molecule in clay’s interlayer). Each pore diffusion is described with a
 154 tortuosity τ (purely geometrical) and a constrictivity δ (which take into account pore section
 155 variability, steric effect, viscosity effect). He considered the same tortuosity for the three
 156 networks. The total diffusion flux is the sum of the fluxes for each pore network.

157 Other authors consider the division of the connected porosity into compartments: one
 158 for the sorbed species and the bulk water. According to Kim et al. (1993) and Eriksen et al.
 159 (1999), these two compartments contain mobile charges. Therefore two diffusion coefficients
 160 have to be considered: the bulk diffusion coefficient D_i and the surface diffusion coefficient

161 D_i^S (in $\text{m}^2 \text{s}^{-1}$). Introducing this surface diffusion coefficient in the constitutive equation
 162 yields,

$$163 \quad \mathbf{J}_i = -[D_i + (1 - \phi)\rho_g K_d^i D_i^S] \nabla C_i. \quad (8)$$

164 This model was used by Muurinen (1994) to model the diffusion of cations in charged porous
 165 media. He found that D_i is generally stronger than D_i^S by at least one order of magnitude.
 166 This result is consistent with the fact that the electromigration mobility of the counterions in
 167 the Stern layer is usually smaller than the mobility of the ions in the bulk pore water by one
 168 order of magnitude (Revil et al., 1998; Revil, 1999). However, there is no reason that surface
 169 diffusion would act in parallel to the bulk diffusion. We know, from electrical conductivity
 170 models, that the electromigration of the ions follows very different paths between the bulk
 171 pore space and the surface of the pores (Bernabé and Revil, 1995). In addition, there is no
 172 clear picture of surface diffusion in the Stern layer. Models for the electromigration of the
 173 counterions in the Stern layer predict no migration of the counterions in this layer at zero
 174 frequency (Leroy et al., 2008). Because of the intrinsic connection between diffusion and
 175 electromigration, this implies that the diffusion of the counterions in the Stern layer is
 176 physically not possible because it is not possible to build surfaces concentration gradients in
 177 the Stern Layer. In addition, the fraction of counterions between the Stern Layer and the
 178 diffuse layer is relatively independent on the salinity of the pore water (see Leroy and Revil,
 179 2004).
 180

181 The main problem with the previous approaches is that they do not take in
 182 consideration the influence of the electrical diffuse layer upon the concentrations of the ionic
 183 species in the micropores (see Leroy et al., 2007). Some diffusion models, however, are
 184 partially based on the properties of the electrical double layer. Several authors proposed to
 185 divide the pore space into three compartments (i) the Stern layer with immobile sorbed ions,
 186 (ii) the diffuse layer with mobile ions (but with concentrations determined by solving the

187 Poisson-Boltzmann differential equation), and (iii) the bulk water of the pore which contains
 188 free ions. Sato et al. (1995) proposed for example to introduce the contribution of ion located
 189 in the diffuse double layer with an electrostatic constrictivity δ_{el} :

$$190 \quad \mathbf{J}_i = -\delta_{el} D_i \nabla C_i. \quad (9)$$

191 This electrostatic constrictivity is the ratio between the average concentration of ion in the
 192 diffuse layer $C_i^d(x)$ and the concentration in the bulk water C_i (Sato et al., 1995),

$$193 \quad \delta_{el} = \frac{1}{RC_i} \int_0^R C_i^d(x) dx, \quad (10)$$

194 where R is the mean pore radius, x is the distance normal to the surface of the pores, and
 195 $C_i^d(x)$ is the local concentration of species i determined by solving the Poisson-Boltzmann
 196 equation at the interface solution scale (local scale). Ochs et al. (2001) used however
 197 electrostatic constrictivity as a fitting parameter. We will show in Section 3 that our approach
 198 yields a much better expression to determine the electrostatic constrictivity, which will be
 199 based on an extension of Donnan equilibrium theory.

200 Molera and Eriksen (2002) use a partition coefficient f between the species located in
 201 the diffuse-layer and those located in the Stern layer. This fraction is assumed to have no
 202 dependence with C_i and C_i^S . This yields another expression for the constitutive equation,

$$203 \quad \mathbf{J}_i = - \left\{ D_i \left[1 + f \frac{(1-\phi)}{\phi} \rho_g K_d^i \right] \right\} \nabla C_i. \quad (11)$$

204 However, they do not provide a way to estimate this parameter from the underlying electrical
 205 double layer theory.

206 In all the models discussed previously, the parameters involved in the generalized
 207 Fick's law (like the electrostatic constrictivity δ or the coefficient f) have to be determined
 208 empirically. In the next section, we use a ionic diffusion model based on a volume averaging
 209 approach of the Nernst-Planck equation and related to the electrical double layer theory (Revil

210 and Linde, 2006). We start with the work of Leroy et al. (2007) who modeled the pore water
 211 composition of the Callovo-Oxfordian argillite (COx) accounting for the micro- and
 212 macroporosity. We extend their work to the modeling of the diffusion of ionic tracers through
 213 clay-rocks. This model will be used to interpret the experimental results obtained by Melkior
 214 et al. (2007) and Bazer-Bachi et al. (2007) who characterize the diffusion of alkaline cations
 215 and anions through Callovo-Oxfordian argillite core samples.

216

217

3. A NEW MODEL

3.1. *Underlying Assumptions*

218

219
 220 In this section, we develop a model for the Cox clay-rock (see Figure 1). We consider
 221 a charged porous medium fully saturated by a multicomponent electrolyte with Q species. In
 222 contact with water, this surface of the solid phase of the clay particles is assumed to carry a
 223 net electrical charge density because of the complexation of the surface sites with the
 224 elements of the pore water and isomorphic substitution in the crystalline framework. This
 225 surface charge density is responsible for the formation of an electrical triple layer (Figure 2)
 226 that includes the Stern layer and the diffuse layer (Hunter, 1981).

227 The electroneutrality of a representative elementary volume of the rock is written as:

$$228 \quad \bar{Q}_v + \frac{S}{V_f} Q_s = 0, \quad (12)$$

229 where \bar{Q}_v is the total charge of the diffuse layer per unit pore volume of the connected
 230 porosity, $Q_s = Q_0 + Q_\beta$ is the total surface charge density (in $C\ m^{-2}$) on the surface of the clay
 231 particles. This charge density includes the charge density due to the active sites covering its
 232 surface Q_0 and the charge density of the Stern Layer Q_β (Figure 2), S (in m^2) is the surface
 233 area of the interface separating the solid and the liquid phases in a representative elementary

234 volume of the material, and V_f is the pore volume (in m^3) of the same representative
 235 elementary volume. The volumetric charge density \bar{Q}_v corresponds to the net amount of
 236 charge of the diffuse layer per unit pore volume (in C m^{-3}). It is defined by:

$$237 \quad \bar{Q}_v = (1 - f_Q) Q_v, \quad (13)$$

238 where f_Q is the fraction of charge carried by the counterions located in the Stern layer or, in
 239 other words, the partition coefficient of the countercharge between the Stern and the diffuse
 240 layers, and Q_v represents the total charge density associated with the cation exchange
 241 capacity of the material (Revil et al., 2002)

$$242 \quad Q_v = \rho_g \left(\frac{1 - \phi}{\phi} \right) \text{CEC}, \quad (14)$$

243 where ρ_g the solid grain density (in kg m^{-3}) and the CEC is the cation exchange capacity of
 244 the medium (in mol kg^{-1}). Using an electrical triple layer model, Leroy et al. (2007) obtained
 245 $f_Q = 0.94 \pm 0.02$ at 25°C for the COx clay-rock. Gonçalvès et al. (2007) obtained $f_Q \approx 0.85$
 246 from filtration efficiency experimental data for a compacted bentonite. This means that a large
 247 fraction of the counterions are located in the Stern layer.

248 In thermodynamic equilibrium, the Donnan equilibrium model is based on the equality
 249 between the electrochemical potential of the ions in the pore space of the charged porous
 250 material and in a reservoir of ions in contact with the charged porous material. In terms of
 251 concentrations, the concentration of the species i in the pore space of the material, \bar{C}_i , is
 252 related to the concentration of the species i in the reservoir, C_i , by (e.g., Revil and Linde,
 253 2006)

$$254 \quad \bar{C}_i = C_i \frac{\gamma_i}{\bar{\gamma}_i} \exp\left(-\frac{q_i \phi_m}{k_B T}\right), \quad (15)$$

255 where $q_i = (\pm e)z_i$ represents the charge of the ion i (in C) with z_i the valence of the ion and e
 256 the elementary charge (1.6×10^{-19} C), k_B the Boltzmann constant (1.381×10^{-23} J K⁻¹), T the
 257 absolute temperature in K, γ_i and $\bar{\gamma}_i$ are the activity coefficients of ion i in the macropores
 258 and micropores, respectively, the ionic concentration in micropores, and φ_m is the mean
 259 electrical potential in the pore space of the medium. Leroy et al. (2007) showed that the ration
 260 of the activity coefficient can be neglected ($\gamma_i / \bar{\gamma}_i \approx 1$).

261 The potential φ_m can be determined from the volumetric charge density \bar{Q}_V by
 262 solving numerically the following charge balance equation (see Revil and Linde, 2006; Leroy
 263 et al., 2007),

$$264 \quad \bar{Q}_V = \sum_{i=1}^Q q_i C_i \exp\left(-\frac{q_i \varphi_m}{k_B T}\right). \quad (16)$$

265 To perform these computations, we need the macropore water composition proposed for
 266 example by the THERMOAR model (Gaucher et al., 2004) at 25°C. Following Leroy et al.
 267 (2007), we took $\text{CEC} = 0.18 \text{ mol kg}^{-1}$, $\rho_g = 2700 \text{ kg m}^{-3}$, $T = 298.15 \text{ K}$ (25°C), and
 268 $f_Q = 0.94 \pm 0.02$. With these parameters, we will show later that the mean electrical potential
 269 of the pore space of the Cox clay-rock is typically in the range from -20 mV to -40 mV.

270 From Eqs. (10) and (15) and using $\gamma_i / \bar{\gamma}_i \approx 1$, the mean electrical potential can be also
 271 related to the electrostatic constrictivity introduced by Sato et al. (1995) (see section 2):

$$272 \quad \delta_{el} = \frac{\bar{C}_i}{C_i} = \exp\left(-\frac{q_i \varphi_m}{k_B T}\right). \quad (17)$$

273 For the COx clay-rock, surface properties are dominated by the reactivity and specific
 274 surface area of smectite. Using the triple layer model, we can determine the distribution
 275 coefficient $K_d^i = C_i^s / C_i$ using the calculated surface site density of sorbed counter-ions in the
 276 Stern layer Γ_{Xi}^0 (in sites m⁻²). The subscript “X” refers to the surface sites resulting from

277 isomorphic substitutions into the mineral lattice and situated on the basal planes of the
 278 smectite particles (Leroy et al., 2007). In most of experimental studies, the distribution
 279 coefficient K_d^i is obtained by batch or column experiment for each type of tracer.

280 The concentration of sorbed species C_i^S is given by:

$$281 \quad C_i^S = \Gamma_{X_i}^0 S_{sp}, \quad (18)$$

282 where S_{sp} is the specific surface (in $\text{m}^2 \text{kg}^{-1}$ of mineral). Gaucher et al. (2004) proposed an
 283 average specific surface for the COx: $S_{sp} = 5 \times 10^4 \text{m}^2 \text{kg}^{-1}$. In the case respectively of
 284 monovalent and bivalent counterions, the surface site density of sorbed counterions in the
 285 Stern layer $\Gamma_{X_i}^0$ is determined by Leroy et al. (2007):

$$286 \quad \Gamma_{X_i}^0 = \frac{\Gamma_X^0 a_i}{K_i} \exp\left(-\frac{e\varphi_\beta}{k_B T}\right), \quad (19)$$

$$287 \quad \Gamma_{X_i}^0 = \frac{\Gamma_X^{0^2} a_i}{-2K_i \frac{Q_0}{e}} \exp\left(-\frac{2e\varphi_\beta}{k_B T}\right), \quad (20)$$

288 where φ_β is the electrical potential at the Stern plane and Γ_X^0 the surface site density of the
 289 “X” sites. Leroy et al. (2007) have determined an average of these two parameters for the
 290 COx medium: $\varphi_\beta = -95.3 \text{mV}$, $\Gamma_X^0 = 9.1 \times 10^{16} \text{sites m}^{-2}$. The parameter a_i is the activity of the
 291 species i in the macropores, Q_0 (in C m^{-2}) the surface charge density at the surface of mineral,
 292 and K_i the speciation constants associated with the adsorption/desorption of the counterion i .
 293 This model will be used to compute a priori value for K_d^{Na} of the $^{22}\text{Na}^+$ tracer in section 5.

294

295 **3.2. A Model for the Diffusion of Tracers**

296

297 We consider the ionic tracer diffusion through the clay-rock. Revil and Linde (2006)
 298 proposed a multi-ionic diffusion model in which flux of species i is driven by the gradient of

299 its electrochemical potential. In the present case, there is no macroscopic electrical field
 300 because of the concentration of the tracer is much smaller than the ionic strength of the pore
 301 water. In appendix A, we show that this model yields an apparent Fick's law,

$$302 \quad \mathbf{J}_i = -D_i \nabla C_i, \quad (21)$$

$$303 \quad D_i = \frac{\beta_i \bar{C}_i k_B T}{q_i C_i F}, \quad (22)$$

304 where D_i is the effective diffusion coefficient of the ionic species in the microporous charged
 305 medium, β_i is the ionic mobility, and F is the electrical formation factor. Note that D_i is the
 306 product of three terms: (i) the self-diffusion of the ionic tracer in the water D_i^f , which is
 307 expressed by the Nernst-Einstein relation,

$$308 \quad D_i^f = \frac{\beta_i k_B T}{q_i}, \quad (23)$$

309 (ii) the electrical formation factor F which can be related to the porosity by Archie's law
 310 $F = \phi^{-m}$ (Archie, 1942), where m is called the cementation exponent and with $1 \leq m \leq 3$ for
 311 most of all media (m has been determined equal to 1.95 ± 0.04 in the COx by Revil et al.,
 312 2005; and comprises between 2 and 3 by Descostes et al., 2008), and (iii) the \bar{C}_i / C_i ratio,
 313 which is given by Eq. (15).

314 From Eqs. (15), (22), and (23), we obtain the following relationship between the
 315 effective diffusion coefficient and the diffusivity:

$$316 \quad \eta_i = \frac{D_i^f}{\phi + (1-\phi)\rho_g K_d^i} \left(\frac{1}{F} \right) \exp\left(-\frac{q_i \varphi_m}{k_B T} \right). \quad (24)$$

$$317 \quad D_i = \frac{D_i^f}{F} \exp\left(-\frac{q_i \varphi_m}{k_B T} \right). \quad (25)$$

318 Therefore the diffusivity of an ionic tracer depends only upon three key-parameters: K_d^i , F ,
 319 and φ_m . The formation factor can be obtained by a variety of methods like the measurement

320 of the electrical conductivity of the porous material at different salinities of the brine to
321 separate the contribution from the brine conductivity from the surface conductivity
322 contribution (note that F is NOT the ratio of the brine conductivity to the effective
323 conductivity of the rock as written in a number of papers). The formation factor can also be
324 obtained by steady-state HTO (tritiated water) diffusion experiments. HTO is considered to be
325 a non-reactive species with the mineral/water interface. Therefore the model of Revil (1999)
326 yields $F = D_{HTO}^f / D_{HTO}$ where D_{HTO}^f is the value of self-diffusion coefficient of HTO in water
327 and D_{HTO} represents the value of the effective diffusion coefficient of HTO through the
328 porous material.

329

330 **4. NUMERICAL SIMULATIONS AND SENSITIVITY ANALYSIS**

331

332 The previous system of equations was solved by a PDE solver based on the finite-
333 element method (the Earth Science module of COMSOL MultiphysicsTM 3.4). We have
334 checked the accuracy of the solver by comparing the results with known analytical solutions
335 (e.g. Crank, 1975). The problem can therefore be solved in 1D, 2D, or 3D accounting for the
336 heterogeneity in the distribution of the material properties (e.g., the formation factor) or the
337 physicochemical parameters associated with the clay content and the clay mineralogy.

338 To keep our numerical test simple in this paper (and to compare our model to
339 experimental data), we consider the 1D problem of a tracer through-diffusion experiment. The
340 through diffusion technique is common laboratory method to determine the diffusion
341 properties of consolidated clay material (e.g., Melkior et al., 2004). A small cylinder of the
342 medium is placed between two reservoirs filled with water in chemical equilibrium with this
343 medium. In order to study diffusion properties of a considered ionic species i , a trace
344 concentration of a radioactive isotope is placed in the upstream reservoir. As the tracer

345 concentration is very low, there is no real concentration gradient in the medium and therefore
 346 no electroosmotic flow and no macroscopic electrical field. Tracer concentrations in each
 347 reservoir are managed and kept as constant as possible: trace concentration in the upstream
 348 reservoir and null in the downstream reservoir. In general, diffusion properties of medium are
 349 determined by tracer influx in the downstream reservoir (Melkior, 2000 and Melkior et al.,
 350 2004). We use constant boundary conditions: $C_T = 10^{-14} \text{ mol m}^{-3}$ (trace level) in the upstream
 351 reservoir and $C_T = 0 \text{ mol m}^{-3}$ in the downstream reservoir (Figure 3). We note L (in m) the
 352 length of the core sample, which is divided into 120 elements.

353 We compute the evolution of normalized ionic fluxes \mathbf{J}_N in the downstream reservoir
 354 as a function of time. The flux of the ionic tracer in the downstream reservoir is normalized by
 355 the tracer concentration in the upstream reservoir and by the length L of the core sample. Thus
 356 the normalized flux \mathbf{J}_N is expressed in $\text{m}^2 \text{ s}^{-1}$. Time axis will be expressed in days for
 357 convenience (the computations are all performed in SI units).

358 We discuss now the sensitivity of the model to its parameters described in section 3.
 359 This synthetic case was implemented with the properties of the COx and the pore water
 360 chemistry obtained by Leroy et al. (2007). The porosity $\phi = 0.164$ yields $F = \phi^{-1.95} = 34.0$.
 361 The density $\rho_g = 2700 \text{ kg m}^{-3}$, the CEC = 0.18 mol kg^{-1} , and the partition coefficient $f_Q = 0.94$
 362 yield $\varphi_m = -14.9 \text{ mV}$ using Eqs. (13)-(16). If the partition coefficient f_Q takes the values 0.92
 363 and 0.96, φ_m is equal to -18 and -11 mV, respectively. We consider a radioactive metal cation
 364 tracer M^+ with a total concentration (tracer and stable isotope) in the medium
 365 $C_{M^+} = 31.5 \times 10^{-3} \text{ mol L}^{-1}$, the mobility $\beta_{M^+} = 5.19 \times 10^{-8} \text{ m}^2 \text{ s}^{-1} \text{ V}^{-1}$ and the following
 366 distribution coefficient $K_d^{M^+} = 10^{-3} \text{ m}^3 \text{ kg}^{-1}$. Figure 4 shows the sensitivity of the model to
 367 these four important parameters.

368 By definition (see section 3), the formation factor F and the electrical mean potential
369 φ_m (which depends on f_Q) influence the effective diffusion coefficient, while the distribution
370 coefficient K_d affects only the apparent diffusion coefficient. Figure 4a, 4b, 4c and 4d show
371 the sensitivity of the model to F , φ_m , f_Q , and K_d respectively. The model is very sensitive to
372 these parameters. Lower is the formation factor F , higher is the diffusion flux. The parameters
373 φ_m and f_Q are related to each other. For a cation, lower is the mean electrical potential φ_m ,
374 higher is the normalized flux.

375

376 5. COMPARISON WITH EXPERIMENTAL DATA

377 5.1. Laboratory Experiments

378

379 The model presented in Section 4 is compared to tracer through-diffusion experiments
380 in Callovo-Oxfordian clay-rock samples. We consider the following tracers (i) $^{22}\text{Na}^+$ (data
381 from Melkior et al., 2007), (ii) $^{36}\text{Cl}^-$, and (iii) $^{35}\text{SO}_4^{2-}$ (data from Bazer-Bachi et al., 2007). The
382 core samples used by these authors have been extracted from different locations in the COx
383 formation. The properties of the core samples are summarized in Table 1. The samples from
384 K100 in Bazer-Bachi et al. (2007) corresponds to an end-member of the overall formation in
385 term of clay content and porosity (see Table 1).

386 Through-diffusion experiments were performed in two different core samples for $^{36}\text{Cl}^-$
387 and $^{35}\text{SO}_4^{2-}$. This could explain the small differences in porosities and formation factors for
388 the two experiments. Experiments were run with a synthetic water of a composition as close
389 as it possible to the chemical equilibrium with the initial medium (see Table 2). Samples were
390 put in contact with this synthetic water for several weeks to reach equilibrium. Diffusion
391 results are presented as normalized ionic out-flux J_N measured in the downstream reservoir

392 versus time. This allows the comparison between results for different values of the thickness
 393 and the diameter of the samples.

394 In order to compare the model with the experimental data, we first determine a priori
 395 values for the three key-parameters (the formation factor, the mean electrical potential of the
 396 pore space, and the sorption coefficients). For each sample, HTO diffusion data are used to
 397 determine the a priori value of the formation factor using $F = D_{HTO}^f / D_{HTO}$. Results are given
 398 in Table 3. Then, from the synthetic porewater composition and the model described in
 399 section 3.1, we determine the a priori, value of the mean electrical potential φ_m (see Eqs 13 to
 400 16). They are given in Table 3 using the value $f_Q = 0.94$ discussed above. We use the
 401 distribution coefficients K_d^i given by Melkior et al. (2007) and Bazer-Bachi et al. (2007) for
 402 each sample. These distribution coefficients have been determined by batch test or column
 403 test experiments. The a priori values of the distribution coefficient of cations (counterions) can
 404 also be obtained from Eq. (18) to (20). Therefore, we will compare this result for $^{22}\text{Na}^+$ in the
 405 sample HTM102 (-464 m deep), to the K_d value obtained by batch experiment from Melkior
 406 et al. (2007).

407 For each data set, we fit the data with the Simplex algorithm (Caceci and Cacheris,
 408 1984) to obtain the a posterior values of the key-parameters F , φ_m , and K_d^i . The forward
 409 problem solved by COMSOL Multiphysics™ 3.4 is coupled to an optimization routine
 410 written in MatLab® routine (Figure 5). Our algorithm looks for the minimum of the cost
 411 function G ,

$$412 \quad \text{Min } G \equiv \sum_{i=1}^N \left| \frac{\mathbf{J}_{N \text{Exp}}^i - \mathbf{J}_{N \text{Model}}^i}{\mathbf{J}_{N \text{Model}}^i} \right| + 2/3 R, \quad (26)$$

$$413 \quad R \equiv \left| \frac{F^{opt} - F^{ap}}{F^{ap}} \right| + \left| \frac{\varphi_m^{opt} - \varphi_m^{ap}}{\varphi_m^{ap}} \right| + \left| \frac{K_d^{opt} - K_d^{ap}}{K_d^{ap}} \right| \quad (27)$$

414 where N is the number of the experimental data i , and R a regularization term (see Tikhonov,
 415 1963). The superscripts “opt” and “ap” mean optimized and a priori parameters, respectively.
 416 Figure 6 shows that the cost function G has an unique minimum.

417 Figure 7 presents fitted formation factors of the investigated samples versus the
 418 porosity. We have also plotted F from bibliographic data on the Callovo-Oxfordian and
 419 Archie’s law $F = \phi^{-m}$ (for $m = 1.95$ and $m = 3$) on this figure to show the consistency of the
 420 fitted values. We notice that $m = 3$ correspond to the proposed value of Mendelson and Cohen
 421 (1982) for long smectite minerals, like montmorillonite. Note that these formation factors
 422 results also from different evaluations: Revil et al. (2005) obtained their formation factors
 423 (Figure 7a) from electrical conductivity measurement at different salinities while the values
 424 proposed by Descostes et al. (2008) are based on HTO diffusion data (Figure 7b).

425 Figure 8 shows the fitted mean electrical potential versus porosity compared to the
 426 model of Revil and Linde (2006) described in Eqs. (13)–(16), using the porewater chemistry
 427 given by the bibliography (Table 2).

428 The distribution coefficient K_d^{Na} studied by Melkior et al. (2007) can be calculated
 429 following our approach by Eq. (18)–(20) and use as an a priori parameter. This computation
 430 use COx parameters: $\varphi_\beta = -95.3 \times 10^{-3}$ V, $\Gamma_x^0 = 9.1 \times 10^{16}$ sites m^{-2} (from Leroy et al., 2007),
 431 and $S_{sp} = 5 \times 10^4$ m^2 kg^{-1} (from Gaucher et al., 2004). Leroy et al. (2007) have also determine
 432 $K_{Na} = 0.80 \pm 0.05$, which is consistent with the value proposed by Avena and De Pauli (1998)
 433 ($K_{Na} = 0.77$). Using the pore water composition proposed by Melkior et al. (2007)
 434 ($C_{Na^+} = 3.44 \times 10^{-3}$ mol L^{-1}), Eq. (19) yields the surface site density of counterions in the Stern
 435 layer equal to $\Gamma_{xNa}^0 = 1.72 \times 10^{17}$ sites m^{-2} .

436

437 *5.1.1. Diffusion of $^{22}Na^+$*

438

439 We ran an optimization for the $^{22}\text{Na}^+$ tracer diffusion data for sample HTM102 (464 m
440 deep) (Melkior et al., 2007). The value of the distribution coefficient they found by a batch
441 experiment is equal to $0.41 \times 10^{-3} \text{ m}^3 \text{ kg}^{-1}$. And using the TLM model of Leroy et al. (2007),
442 we determine an a priori value of $K_d^{\text{Na}^+} = 0.414 \times 10^{-3} \text{ m}^3 \text{ kg}^{-1}$ which corresponds to an
443 excellent agreement between the TLM model and the experimental value by a batch
444 experiment. A priori values for the formation factor and the mean electrical potential are
445 $F = 89.6$ and $\varphi_m = -23.2 \text{ mV}$, respectively.

446 The fitted normalized flux curve and experimental data are presented in Figure 9. The
447 best fit yields the following a posteriori values: $F = 82.6$, $\varphi_m = -23.5 \text{ mV}$, and $K_d = 0.704 \times 10^{-3}$
448 $\text{ m}^3 \text{ kg}^{-1}$. The correlation coefficient between the fitted model and experimental data is very
449 good ($R^2 = 97.4 \%$). The fitted and the computed formation factor F are very close
450 ($RE = 7.9 \%$). The mean electrical potential fitted corresponds pretty well to the computed one
451 ($RE = 2.6 \%$). But the distribution coefficient presents a difference but is still acceptable
452 ($RE = 41.8 \%$). The differences seen between fitted and computed parameters can easily be
453 explained by both the uncertainties on the experimental data, the porosity, and the value of F
454 resulting from HTO diffusion data.

455

456 5.1.2. Diffusion of ^{36}Cl

457

458 We ran the simulation for $^{36}\text{Cl}^-$ tracer diffusion in the EST205 K100. Figure 10 shows
459 the confrontation between the fitted normalized diffusion flux following our model and
460 experimental data from Bazer-Bachi et al (2007). The chloride $^{36}\text{Cl}^-$ is a non-sorbed tracer, so
461 we consider $K_d = 0 \text{ m}^3 \text{ kg}^{-1}$. The other a priori value are $F = 772.3$ and $\varphi_m = -32.1 \text{ mV}$.

462 The minimization of the cost function G yields the following a posteriori values of the
463 model parameters: $F = 772.3$ and $\varphi_m = -47.0$ mV ($R^2 = 75.5$ %). Computed and fitted
464 formation factor F are equal but the a posteriori value of mean electrical potential φ_m presents
465 a slight difference with the a priori value ($RE = 46.9$ %).

466

467 5.1.3. Diffusion of $^{35}\text{SO}_4^{2-}$

468

469 We have also simulated the $^{35}\text{SO}_4^{2-}$ diffusion data through a clay-rock sample from the
470 EST205 K100 core (Bazer-Bachi et al., 2007). As SO_4^{2-} can be sorbed onto the mineral
471 surface (Bazer-Bachi et al., 2007; Descostes et al., 2008), Bazer-Bachi et al. (2007) have
472 performed a column test to determine the value of this parameter. They found $K_d = 1.80 \times 10^{-5}$
473 $\text{m}^3 \text{kg}^{-1}$. The a priori values of formation factor and mean electrical potential are $F = 717.1$
474 and $\varphi_m = -29.1$ mV, respectively.

475 The minimization of the cost function G yields the following a posteriori values:
476 $F = 718.3$, $\varphi_m = -29.2$ mV, and $K_d = 1.60 \times 10^{-5} \text{m}^3 \text{kg}^{-1}$ ($R^2 = 46.9$ %) (Figure 11). The strong
477 dispersion of the experimental data yields a low R^2 fit value. However, the fitted and
478 computed formation factors F are very close to each other ($RE = 0.2$ %). The same applies for
479 the mean electrical potential ($RE = 0.3$ %). The fitted K_d is also pretty close from the value
480 resulting from the column experiment ($RE = 12.5$ %).

481

482 5.2. Field Data

483

484 In a recent study, Descostes et al. (2008) determined the diffusion coefficients of
485 several anions (Cl^- , I^- , SO_4^{2-} , and SeO_3^{2-}) in a set of the Callovo-Oxfordian clay-rock samples
486 formation and in the Oxfordian limestones which is formation lying just above the Cox

487 formation in the Paris Basin. From the top of the Oxfordian formation to 399 m deep, the
 488 formation is composed by several calcareous facies (called C3b, L1a, L1b, L2a, L2b, L2c)
 489 with 80 to 95 % of carbonates (ANDRA, 2005). Then, between 399 and 417 m deep, the
 490 Oxfordian present important vertical mineralogy variations (facies C3a). The carbonate
 491 fraction decreases roughly from 80 % (399 m deep) to less than 40 % (417 m deep) while the
 492 clay fraction increase from 15 % to 45 % (illite, mica and interstratified illite/smectite). The
 493 rest contains principally by quartz. The upper part the COx formation (facies C2d, 417-437 m
 494 deep) presents important spatial variations of mineralogy in the same order of magnitude
 495 than C3a. Then below 437 m deep, the COx become more homogeneous with 40 to 50 % of
 496 clay minerals, 20-35 % of carbonates and 35-25 % of quartz (facies C2b1, C2b2, and C2c)
 497 (ANDRA, 2005).

498 The measurements of the diffusion coefficients were performed with the through-
 499 diffusion technique using a collection of core samples at depths from 166 m to 477 m. For
 500 each sample where anionic diffusion was made, except for SeO_3^- , the HTO diffusion
 501 coefficient was also measured. We use first the HTO diffusion coefficients to determine the
 502 values of the formation factor $F = D_{HTO}^f / D_{HTO}$ (see Figure 7b). Then, using Eq. (23), we
 503 determine the mean electrical potential φ_m from F and D_i :

$$504 \quad \varphi_m = -\frac{k_B T}{q_i} \log\left(\frac{D_i F}{D_i^f}\right). \quad (28)$$

505 Figure 12 shows the values of F and φ_m as a function of depth. The calculated
 506 formation factor in the upper part of the Oxfordian limestone formation is quite low (from 177
 507 to 360 m deep), then it becomes more important and reach 10^3 between 400 and 425 m just
 508 above the Callovo-Oxfordian argillites. The C3a layer has been particularly studied by
 509 Descostes et al. (2008) with six samples between 399 and 417 m deep. In the middle of the
 510 COx formation, F is comprised between 40 and 140, which is consistent with the electrical

511 conductivity measurements presented by Revil et al. (2005) and performed at different
512 salinities with NaCl brines.

513 The values of φ_m are very low in the Oxfordian limestone formation. In this formation,
514 we have,

$$515 \quad \lim_{\varphi_m \rightarrow 0} D_i / D_i^f = 1/F, \quad (29)$$

516 which means that the electrostatic constrictivity δ_{el} is equal to one. The C3a layer (399 to
517 417 m deep) presents more important values of the mean potential in the microporosity φ_m .
518 The values of φ_m are in the range between -40 mV to -20 mV.

519 In the COx formation, the calculated mean electrical potential is comprised between -
520 56 mV and -23 mV. Considering the experimental uncertainties and the local variation of
521 parameters (ϕ , CEC) between two samples, the computed φ_m are quite consistent with the
522 average of computed electrical potential: -40.7 mV in the COx. This electrical potential value
523 appears to be stronger than the model predictions by Eqs. (13)-(16).

524 Our tracer diffusion model is directly related to the generalised transport model in
525 microporous media described by Revil and Linde (2006). That implies that parameters like the
526 electrical factor F and the mean electrical potential in the diffuse layer φ_m , can be applied to
527 determine some other rock properties. The osmotic pressure in a medium is one of them.
528 Therefore, in order to test further the range of computed φ_m values, we have decided to
529 compute the value of the osmotic pressure in the COx from the diffusion test data. Revil and
530 Linde (2006) proposed the following relationship between the mean electrical potential φ_m
531 and the osmotic pressures π_m in a microporous medium:

$$532 \quad \pi_m = k_B T \sum_{i=1}^Q C_i \left[\exp\left(-\frac{q_i \varphi_m}{k_B T}\right) - 1 \right]. \quad (30)$$

533 Considering the pore water presented in Descostes et al. (2008), it becomes possible to
534 determine π_m in the COx at several depth from the previously determined φ_m by Eq. (28) and

535 to show them on Figure 13. The predicted values can be compared to the measured fluid
536 overpressure (above the hydrostatic level) in the Callovo-Oxfordian argillites layer (see
537 Gueutin et al., 2007). The measured excess hydraulic heads are in the range 20–60 m (0.2 to
538 0.6 MPa). Comparison between measured overpressure and computed osmotic pressure π_m in
539 the medium are displayed on Figure 13. The computed ϕ_m from Cl^- and SO_4^{2-} diffusion tests
540 (Descostes et al., 2008) are in a fairly good agreement with the measured overpressures. This
541 result will be explored further in a future work but it shows the model presented by Revil et
542 Linde (2006) can explain very different material properties inside a unified framework.

543

544

6. CONCLUSION

545

546 We have used a model based on a volume-average of the Nernst-Planck equation to
547 model the diffusion of ionic tracers ($^{22}\text{Na}^+$, $^{36}\text{Cl}^-$, $^{35}\text{SO}_4^{2-}$) through the Callovo-Oxfordian clay-
548 rock. The model developed by Revil and Linde (2006) is used to compute the diffusion of
549 tracers in these materials using a generalized Donnan equilibrium model and the electrical
550 formation factor. This model is able to explain tracer diffusion experiments performed by
551 different authors in the COx formation and to determine the profile of these parameters in the
552 formations. In addition, the mean electrical potential allows the determination of the osmotic
553 pressure in the medium. The next step will be to develop this model to unsaturated conditions
554 and to connect this diffusion model to geophysical measurements of complex resistivity such
555 as modeled recently by Leroy et al. (2008).

556

557 **Acknowledgement.** We thank the French National Research Council (CNRS) and the French
558 National Agency for Radioactive Waste Management (ANDRA) (S. Altmann and D. Coelho)

559 for their support. J. Lancelot is thanked for his support through the GDR FORPRO. The Ph.D.
 560 thesis of Damien Jougnot is supported by ANDRA. A. Revil strongly thanks T. Young for his
 561 support at CSM. D. Jougnot thanks A. Jardani J.C. Robinet. This paper is Contribution
 562 FORPRO 2008/XXX.

563

564 **Appendix A**

565 In this Appendix, we estimate the influence of the activity coefficient upon the
 566 diffusion of the tracers through a clay-rock. From Revil and Linde (2006), the constitutive
 567 equation of the diffusion flux of a single ion is written as:

$$568 \quad \mathbf{J}_i = -\frac{\bar{\sigma}_i}{q_i^2 F} \nabla \mu_i \quad (\text{A1})$$

569 with F , the formation factor, $q_i = (\pm e)z_i$, the charge of species i and z_i its valence ($e = 1.6 \times 10^{-19}$
 570 C is the elementary charge), and $\bar{\sigma}_i = \beta_i \bar{C}_i q_i$ the contribution of species i to the overall
 571 electrical conductivity of the pore water defined from β_i the ionic mobility and \bar{C}_i the
 572 concentration of species i in the pore space. The chemical potential μ_i is related to the ionic
 573 activity a_i by $\mu_i = k_B T \ln a_i$. This yields,

$$574 \quad \mathbf{J}_i = -\frac{k_B T \beta_i \bar{C}_i}{q_i F} \nabla \ln a_i. \quad (\text{A2})$$

575 The Fick law defines the ionic flux as a function of the concentration gradient. The
 576 relationship between the activity and the concentration is $a_i = \gamma_i C_i$ where γ_i is the activity
 577 coefficient. This yields,

$$578 \quad \nabla \ln a_i = \frac{\nabla(\gamma_i C_i)}{\gamma_i C_i} = \frac{\nabla C_i}{C_i} \left(1 + \frac{C_i}{\gamma_i} \frac{d\gamma_i}{dC_i} \right). \quad (\text{A3})$$

579 From (A1) to (A3), we obtain,

580
$$\mathbf{J}_i = -\frac{k_B T \beta_i \bar{C}_i}{q_i F C_i} (1 + \varepsilon) \nabla C_i, \quad (\text{A4})$$

581
$$\varepsilon \equiv \frac{C_i}{\gamma_i} \frac{d\gamma_i}{dC_i} = C_i \frac{d \ln \gamma_i}{dC_i}. \quad (\text{A5})$$

582 where ε is a correction term. For a ionic strength I lower than 0.5 mol L^{-1} , γ_i can be computed
583 by the Davies equation:

584
$$\log_{10} \gamma_i = -\frac{1}{2} z_i^2 \left(\frac{\sqrt{I}}{1 + \sqrt{I}} - 0.3I \right). \quad (\text{A6})$$

585 This yields,

586
$$\varepsilon = -\frac{\ln 10}{2} z_i^2 C_i \left[\frac{d}{dI} \left(\frac{\sqrt{I}}{1 + \sqrt{I}} \right) - 0.3 \right] \frac{dI}{dC_i}, \quad (\text{A7})$$

587
$$\varepsilon = -\frac{\ln 10}{2} z_i^2 C_i \left[\frac{1}{2\sqrt{I}(1 + \sqrt{I})^2} - 0.3 \right] \frac{dI}{dC_i}. \quad (\text{A8})$$

588 From the definition of the ionic strength,

589
$$I \equiv \frac{1}{2} \sum_{k=1}^Q z_k^2 C_k, \quad (\text{A9})$$

590
$$\frac{dI}{dC_i} = \frac{1}{2} z_i^2. \quad (\text{A10})$$

591 The correction parameter becomes:

592
$$\varepsilon = -\frac{\ln 10}{4} z_i^4 C_i \left[\frac{1}{2\sqrt{I}(1 + \sqrt{I})^2} - 0.3 \right] \quad (\text{A11})$$

593 The correction term $(1 + \varepsilon)$ in Eq. (A5) is always negligible $\varepsilon \ll 1$ when the ionic strength is
594 close to 0.1 mol L^{-1} and bigger. Neglecting the term ε , Eq. (A3) yields an apparent Fick's law,

595
$$\mathbf{J}_i = -\frac{\beta_i \bar{C}_i k_B T}{q_i C_i F} \nabla C_i. \quad (\text{A12})$$

596

597 **References**

- 598 ANDRA (2005) Dossier 2005 argile—Référentiel du site Meuse/Haute-Marne, International
599 report ANDRA n°C.RP.ADS.04.0022.
- 600 Appelo C.A.J., Wersin P. (2007) Multicomponent diffusion modeling in clay systems with
601 application to the diffusion of Tritium, Iodide, and Sodium in Opalinus Clay. *Environ. Sci.*
602 *Technol.* **41**, 5002 -5007.
- 603 Archie G.E. (1942) The electrical resistivity log as an aid in determining some reservoir
604 characteristics. *Trans. AIME* **146**, 54–62.
- 605 Avena M.J., De Pauli C.P. (1998) Proton adsorption and electrokinetics of an Argentinean
606 montmorillonite. *J. Colloid Interface Sci.* **202**, 195–204.
- 607 Bazer-Bachi F., Tevissen E., Descostes M., Grenut B., Meier P., Simonnot M.-O., Sardin M.
608 (2005) Characterization of iodide retention on Callovo-Oxfordian argillites and its
609 influence on iodide migration. *Phys. Chem. Earth* **31**, 517–522.
- 610 Bazer-Bachi F., Descostes M., Tevissen E., Meier P., Grenut B., Simonnot M.-O., Sardin M.
611 (2007) Characterization of sulphate sorption on Callovo-Oxfordian argillites by batch,
612 column and through-diffusion experiments. *Phys. Chem. Earth* **32**, 552–558.
- 613 Bernabé Y., Revil A. (1995) Pore-scale heterogeneity, energy dissipation and the transport
614 properties of rocks. *Geophys. Res. Lett.* **22**(12), 1529-1552.
- 615 Bourg I.C., Bourg A.C.M., Sposito G. (2003) Modeling diffusion and adsorption in
616 compacted bentonite: a critical review. *J. Contam. Hydrol.* **61**, 293–302.
- 617 Bourg I.C. (2004) Caractérisation du comportement d'une bentonite sodique pour l'isolement
618 des déchets : Transport diffusif des traceurs ioniques (Na⁺, Sr²⁺, Cs⁺ et Cl⁻) dans la
619 bentonite sodique compactée saturée, et titration acide-base de la montmorillonite. Ph.D.
620 thesis, Université de Pau et des Pays d'Adour, Pau.
- 621 Bourg I.C., Sposito G., Bourg A.C.M. (2006) Tracer diffusion in compacted, water-saturated
622 bentonite. *Clays and Clay Minerals* **54**, 363–374.
- 623 Caceci M., Cacheris W.P. (1984) Fitting curves to data. The simplex algorithm is the answer.
624 *Byte* **9**, 340–362.

- 625 Chatterji S. (2004) Ionic diffusion through thick matrices of charged particles. *J. Colloid*
626 *Interface Sci.* **269**, 186-191.
- 627 Descostes M., Blin V., Bazer-Bachi F., Meier P., Grenut B., Radwan J., Schlegel M.L.,
628 Buschaert S., Coelho D., Tevissen E. (2008) Diffusion of anionic species in Callovo-
629 Oxfordian argillites and Oxfordian limestones (Meuse/Haute-Marne, France). *Appl.*
630 *Geochem.* **23**, 655–677.
- 631 Eriksen T.E., Jansson M., Molera M. (1999) Sorption effects on cation diffusion in compacted
632 bentonite. *Eng. Geol.* **54**, 231–236.
- 633 Escoffier S., Homand F., Giraud A. (2000) Perméabilité et coefficient de Biot des argilites de
634 MHM, in *Recherches pour le Stockage des Déchets Radioactifs à Haute Activité et à Vie*
635 *Longue, Bilan des Etudes et Travaux 2000* (eds. The French Nuclear Waste Agency) 206-
636 216.
- 637 Gasc-Barbier M., Chanchole S., Bérest P. (2004) Creep behavior of Bure clayey rock. *Appl.*
638 *Clay Sci.* **26**, 449-458.
- 639 Gaucher E., Robelin C., Matray J.M., Negrel G., Gros Y., Heitz J.F., Vinsot A., Rebours H.,
640 Cassabagnere A., Bouchet A. (2004) ANDRA underground research laboratory:
641 interpretation of the mineralogical and geochemical data acquired in the Callovo-
642 Oxfordian Formation by investigative drilling. *Phys. Chem. Earth* **29**, 55–77.
- 643 Gaucher E., Blanc P., Barot F., Braibant G., Buschaert S., Crouzet C., Gautier A., Girard J.P.,
644 Jacquot E., Lassin A., Negrel G., Tournassat C., Vinsot A., Altmann S. (2006) Modeling
645 the porewater chemistry of the Callovo-Oxfordian formation at a regional scale. *C. R.*
646 *Geosciences* **338** (12–13), 917–930.
- 647 Gonçalves J., Rousseau-Gueutin P., Revil A. (2007) Introducing interacting diffuse layers in
648 TLM calculations: A reappraisal of the influence of the pore size on the swelling pressure
649 and the osmotic efficiency of compacted bentonites. *J. Colloid Interface Sci.* **316**, 92-99.
- 650 Gueutin P., Altmann S., Gonçalves J., Cosenza P., Violette S. (2007) Osmotic interpretation
651 of overpressures from monovalent based triple layer model, in the Callovo-Oxfordian at
652 the Bure site. *Phys. Chem. Earth* **32**, 434–440.

- 653 Hunter R.J. (1981). *Zeta Potential in Colloid Science: Principles and Applications*. Academic
654 Press, New York.
- 655 Jacquot E. (2002) Composition des eaux interstitielles des argilites du Callovo-Oxfordien non
656 perturbées: état de la modélisation à Juillet 2002. *ANDRA Report D NT ASTR 02-041*.
- 657 Kim H., Suk T., Park S., Lee C. (1993) Diffusivities for ions through compacted Na-bentonite
658 with varying dry bulk density. *Waste Manag.* **13**, 303–308.
- 659 Crank. J. (1970) *The Mathematics of Diffusion*. Clarendon Press, Oxford.
- 660 Leroy P., Revil A. (2004) A triple-layer model of the surface electrochemical properties of
661 clay minerals. *J. Colloid Interface Sci.* **270** (2), 371–380.
- 662 Leroy P., Revil A., Coelho D. (2006) Diffusion of ionic species in bentonite. *J. Colloid*
663 *Interface Sci.* **296** (1), 248–255.
- 664 Leroy P., Revil A., Altmann S., Tournassat C. (2007) Modeling the composition of the pore
665 water in a clay-rock geological formation (Callovo-Oxfordian, France). *Geochim. et*
666 *Cosmochim. Acta* **71** (5), 10.1016/j.gca.2006.11.009, 1087-1097.
- 667 Leroy P., Revil A., Kemna A., Cosenza P., Ghorbani A. (2008) Complex conductivity of
668 water-saturated packs of glass beads. *J. Colloid Interface Sci.* **321**, 103–117.
- 669 Limousin G., Gaudet J.-P., Charlet L., Szenknect S., Barthès V., Krimissa M. (2007) Sorption
670 isotherms: A review on physical bases, modeling and measurement. *Appl. Geochem.* **22**,
671 249-275.
- 672 Linde N., Jougnot D., Revil A., Matthäi S., Arora T., Renard D., Doussan C. (2007)
673 Streaming current generation in two phase flow conditions, *Geophys. Res. Lett.* **34**,
674 L03306, doi:10.1029/2006GL028878.
- 675 Malusis M.A., Shackelford C.D., Olsen H.W. (2003) Flow and transport through clay
676 membrane barriers. *Eng. Geol.* **70**, 235-248.
- 677 Melkior T. (1999) Etude méthodologique de la diffusion de cations interagissants dans des
678 argiles. Ph.D. Thesis. Ecole Centrale de Paris.
- 679 Melkior T., Mourzagh D., Yahiaoui S., Thoby D., Alberto J.C., Brouard C., Michau N. (2004)
680 Diffusion of an alkaline fluid through clayey barriers and its effect on the diffusion
681 properties of some chemical species. *Appl. Clay Sci.* **26**, 99–107.

- 682 Melkior T., Yahiaoui S., Motellier S., Thoby D., Tevissen E. (2005) Cesium sorption and
683 diffusion in Bure mudrock samples. *Appl. Clay Sci.* **29**, 172–186.
- 684 Melkior T., Yahiaoui S., Thoby D., Motellier S., Barthes V. (2007) Diffusion coefficients of
685 alkaline cations in Bure mudrock. *Phys. Chem. Earth* **32**, 453–462.
- 686 Mendelson K.S., Cohen M.H. (1982) The effect of grain anisotropy on the electrical
687 properties of sedimentary rocks. *Geophysics* **47**, 257–263.
- 688 Molera M., Eriksen T. (2002) Diffusion of $^{22}\text{Na}^+$, $^{85}\text{Sr}^{2+}$, $^{134}\text{Cs}^+$ and $^{57}\text{Co}^{2+}$ in bentonite clay
689 compacted to different densities: experiments and modeling. *Radiochim. Acta* **90**, 753–
690 760.
- 691 Muurinen A., Penttilä-Hiltunen P., Uusheimo K. (1988) Diffusion of chloride and uranium in
692 compacted sodium bentonite. In *Scientific Basis of Nuclear waste Management XII* (Eds.
693 Lutze W. and Erwing R.C.), Materials Research Society, Pittsburg, PA, 743-748.
- 694 Muurinen A. (1994) Diffusion of anions and cations in compacted sodium bentonite. *VTT*
695 *Publication* **168**, Espoo Technical Centre, Finland.
- 696 Ochs M., Lothenbach B., Wanner H., Sato H., Yui M. (2001) An integrated sorption–
697 diffusion model for the calculation of consistent distribution and diffusion coefficients in
698 compacted bentonite. *J. Contam. Hydrol.* **47**, 283–296.
- 699 Revil A., Cathles L.M., Losh S., Nunn J.A. (1998) Electrical conductivity in shaly sands with
700 geophysical applications. *J. Geophys. Res.* **103**, 23,925–23,936.
- 701 Revil A. (1999) Ionic diffusivity, electrical conductivity, membrane and thermoelectric
702 potentials in colloids and granular porous media: A unified model. *J. Colloid Interface*
703 *Sci.* **212**, 503– 522.
- 704 Revil, A., Hermitte, D., Spangenberg, E., Cochémé J.J. (2002) Electrical properties of
705 zeolitized volcanoclastic materials. *J. Geophys. Res.* **107** (B8), 2168.
706 doi:10.1029/2001JB000599.
- 707 Revil, A., Leroy P. (2004) Governing equations for ionic transport in porous shales. *J.*
708 *Geophys. Res.* **109**, B03208, doi : 10.1029/2003JB002755, 2004.

- 709 Revil A., Leroy P., Titov K. (2005) Characterization of transport properties of argillaceous
710 sediments. Application to the Callovo- Oxfordian Argillite. *J. Geophys. Res.* **110**, B06202.
711 doi:10.1029/2004JB003442.
- 712 Revil A., Linde N. (2006) Chemico-electromechanical coupling in microporous media. *J.*
713 *Colloid Interface Sci.* **302**, 682–694.
- 714 Revil A., Linde N., Cerepi A., Jougnot D., Matthäi S., Finsterle S. (2007) Electrokinetic
715 coupling in unsaturated porous media. *J. Colloid Interface Sci.* **313**(1), 315-327,
716 10.1016/j.jcis.2007.03.037.
- 717 Revil, A. (2007) Thermodynamics of transport of ions and water in charged and deformable
718 porous media. *J. Colloid Interface Sci.* **307**(1), 254-264.
- 719 Revil A., Jougnot D. (2008), Diffusion of ions in unsaturated porous materials, *J. Colloid*
720 *Interface Sci.* **319**(1), 226-235, doi: 10.1016/j.jcis.2007.10.041.
- 721 Sato H., Yui M., Yoshikawa H. (1995) Diffusion behavior for Se and Zr in sodium-bentonite.
722 *Materials Research Society Symposium Proceedings* **353**, 269–276.
- 723 Soudek A., Jankhe F.M., Radke C.J. (1983) Ion exchange equilibria and diffusion in
724 engineered backfill. NUREG CP-0052, *Proceedings of the US Nuclear Regulatory*
725 *Comission.* NUREG, Washington, D.C.. 171-203.
- 726 Tikhonov, A. N. (1963) Resolution of ill-posed problems and the regularization method (in
727 Russian), Dokl. Akad. Nauk SSSR, **151**, 501–504.
- 728 Van Brakel J., Heertjes P.M. (1974) Analysis of diffusion in macroporous media in terms of a
729 porosity, a tortuosity, and a constrictivity factor. *Int. J. Heat Mass Transfer* **17**, 1093–
730 1103.
- 731

732 **Table 1.** Physical and chemical characteristics of the through-diffusion samples

	HTM102 (-464m)	EST205 K100
Porosity, ϕ [-]	0.15	0.030 / 0.037 ^a
Grain density, ρ_g [kg m ⁻³]	2670	2700 ^b
Cation exchange capacity		
CEC [meq g ⁻¹]	0.18 ± 0.04 ^c	0.111 ± 0.03 ^d
Temperature, T [K]	296.15 (23°C)	294.15 (21°C)
Depth [m]	464	424
Lithofacies	C2b2	C2d

733 (a) HTO apparent porosity for tracer ³⁶Cl⁻ / ³⁵SO₄²⁻ disk respectively

734 (b) Leroy et al. (2007)

735 (c) Gaucher et al. (2004), Leroy et al. (2007)

736 (d) ANDRA (2005)

737

738

739

740

741

742

743

744

745

746 **Table 2.** Ionic compositions of the synthetic ground water

	Concentration [mol L ⁻¹]	
	<i>Melkior et al. (2007)</i>	<i>Bazer-Bachi et al. (2007)^a</i>
Na ⁺	3.44×10 ⁻²	4.17×10 ⁻²
K ⁺	1.34×10 ⁻⁴	5.40×10 ⁻³
Ca ²⁺	2.87×10 ⁻³	9.74×10 ⁻³
Mg ²⁺	5.26×10 ⁻³	7.68×10 ⁻³
Cl ⁻	5.00×10 ⁻²	7.19×10 ⁻²
SO ₄ ²⁻	7.00×10 ⁻⁵	4.40×10 ⁻³
HCO ³⁻	6.20×10 ⁻⁴	1.44×10 ⁻³
I ^(b)	5.70×10 ⁻²	1.03×10 ⁻¹
pH	8.0	7.2

747 (a) from Jacquot (2002)

748 (b) Ionic strength

749

750 **Table 3.** Computed a priori parameters for tracer diffusion simulation

	Tracer	Porosity, ϕ [-]	Formation factor, F [-]	Electrical mean potential, φ_m [V]	Distribution coefficient, K_d [m ³ kg ⁻¹]
HTM102 (-464m)	²² Na ⁺	0.150	89.6	-23.2×10 ⁻³	0.41×10 ⁻³ ^a
EST205 K100	³⁶ Cl ⁻	0.030 ^b	772.3	-32.1×10 ⁻³	0
	³⁵ SO ₄ ²⁻	0.037 ^b	717.1	-29.1×10 ⁻³	0.018×10 ⁻³ ^c

751 (a) Measured by batch experiment by Melkior et al. (2007)

752 (b) Apparent porosity from HTO diffusion

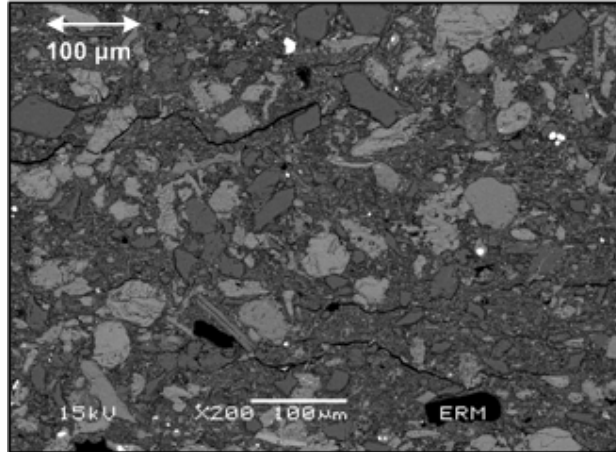
753 (c) Measured by column experiment by Bazer-Bachi et al. (2007)

754

755 **Figure 1.** Picture of a COx sample by scanning electron microscopy (credit: J.C. Robinet).

756 The silica and carbonate grains are embedded into a clay matrix.

757

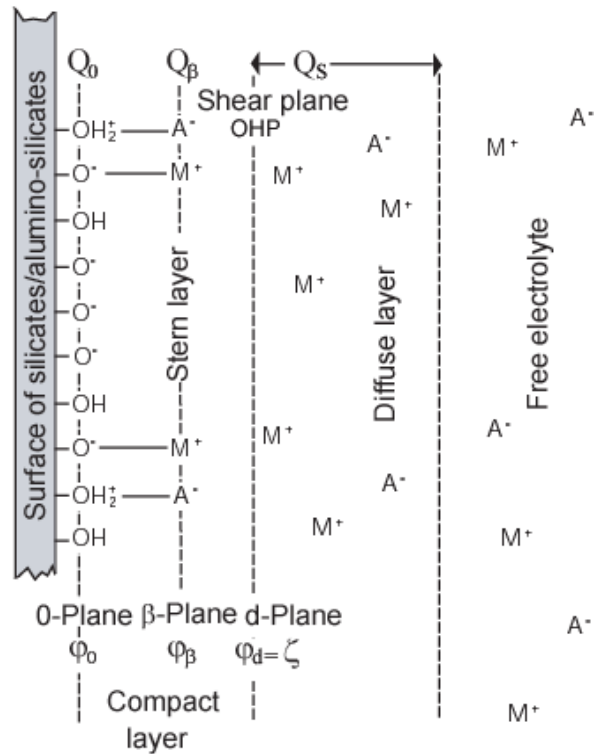


758

759

760

761 **Figure 2.** A charged porous material: the Callovo-Oxfordian clay-rock. (a) Sketch of the COx
 762 at a micro scale. This medium comprises a macroporosity space around grains (e.g. carbonates
 763 and quartz) isolated by microporosity induced by clay minerals. (b) Sketch of the electrical
 764 triple layer extending from the surface of the clay minerals to the center of the pore. M^+
 765 represents metal cations and A^- the anions.
 766



767

768

769

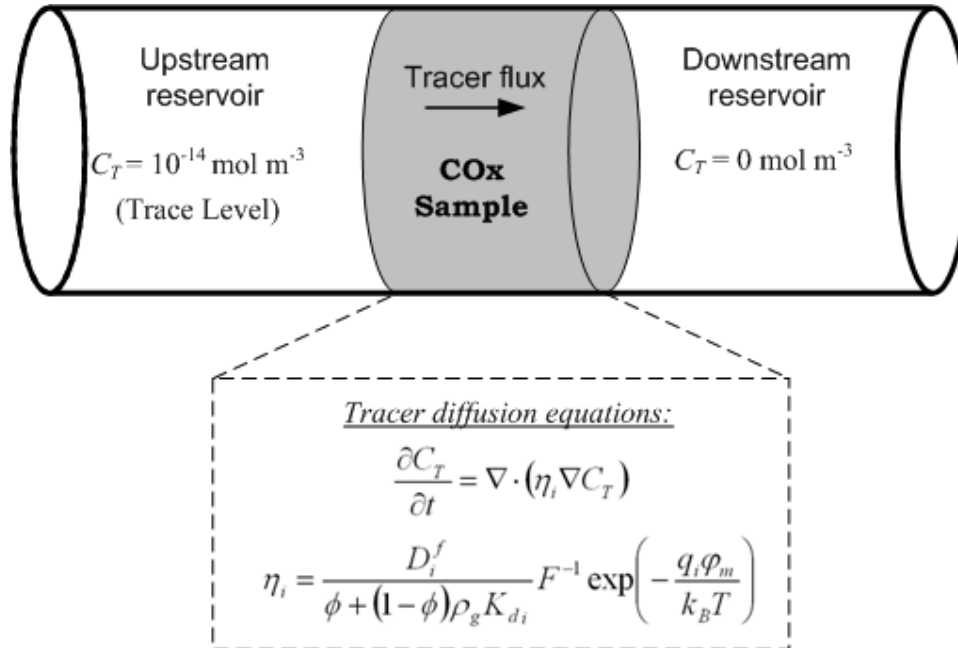
770

771

772

773 **Figure 3.** Implementation sketch of our model for tracer diffusion simulation. The subscripts i
 774 and T refer for the considered ionic species and the used tracer isotope.

775

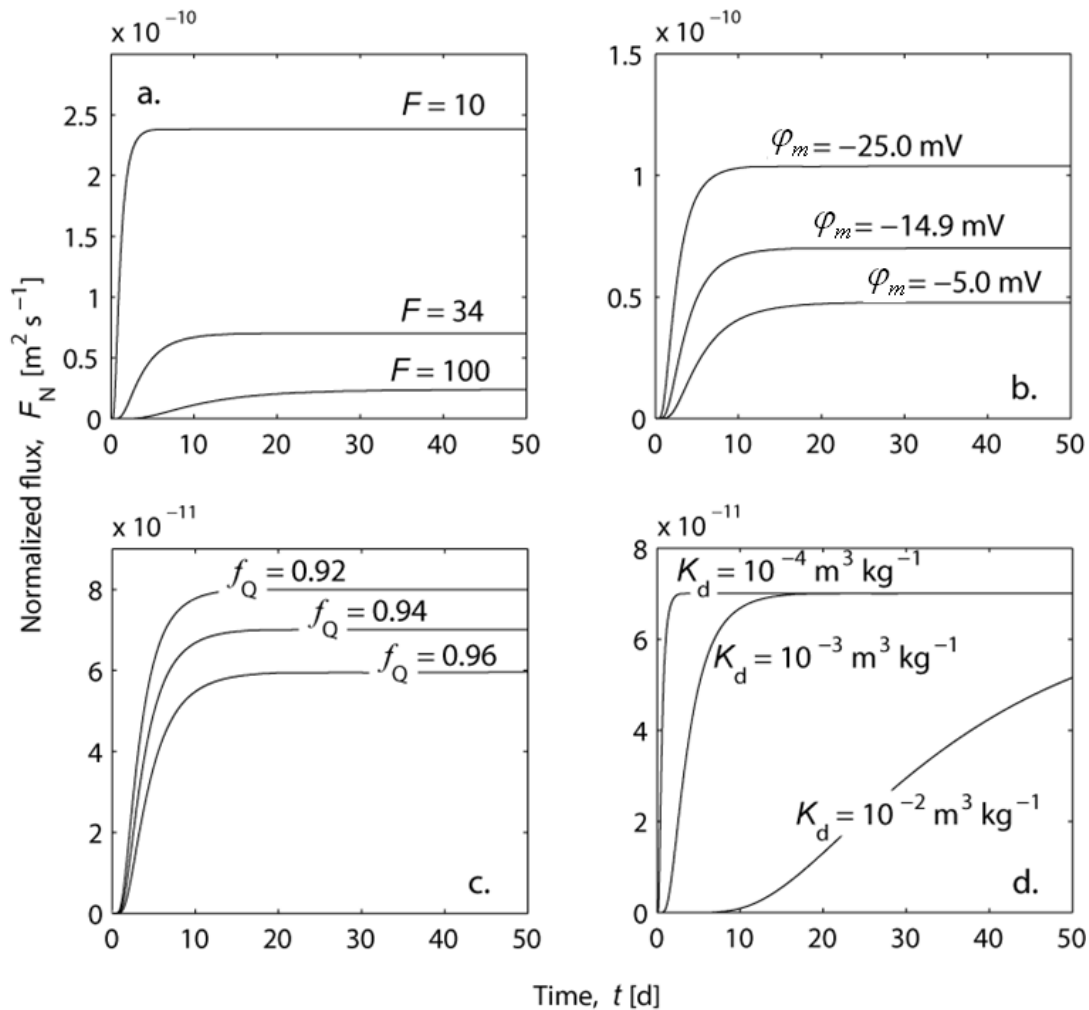


776

777

778

779 **Figure 4.** Model sensitivity of four important parameters on the normalized diffusion flux \mathbf{J}_N
 780 expressed as a function of time (in days, d): (a.) influence of the formation factor F , (b.)
 781 influence of the mean electrical potential φ_m in the microporosity (c.) Influence of the
 782 partition coefficient f_Q of the countercharge between the Stern and the diffuse layers, and (d.)
 783 Influence of the distribution coefficient K_d . Note that in the steady-state regime, the
 784 normalized flux is independent of the value of K_d . The value of K_d influences the
 785 characteristic time of the transient period but not the steady state value of the flux.
 786



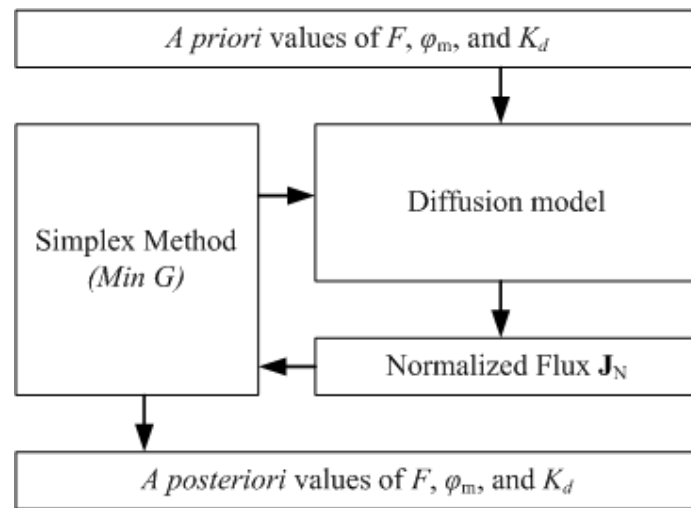
787

788

789

790 **Figure 5.** Optimization algorithm for model parameters determination from experimental
791 normalized flux. The COMSOL multiphysicsTM program provides the normalized diffusion
792 flux data and the Simplex algorithm minimize a cost function G to fit of these data, and then
793 determine the best value of the formation factor, the mean electrical potential in the
794 microporosity, and the partition coefficient for sorption.

795



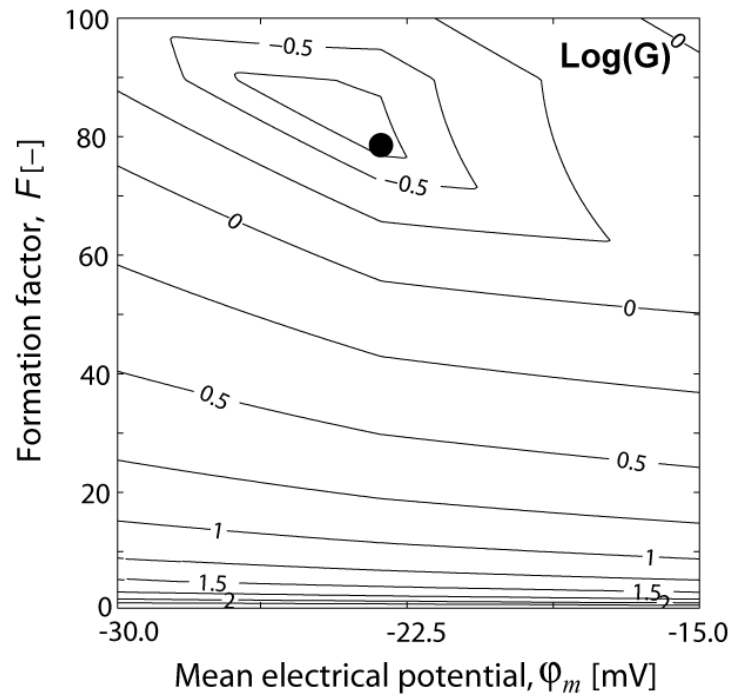
796

797

798

799 **Figure 6.** Shape of the logarithm of the cost function with a regularization term for the
800 optimization of the $^{22}\text{Na}^+$ diffusion experiment (HTM102 -464 m). The cost function G has a
801 unique minimum corresponding to the position of the filled circle.

802

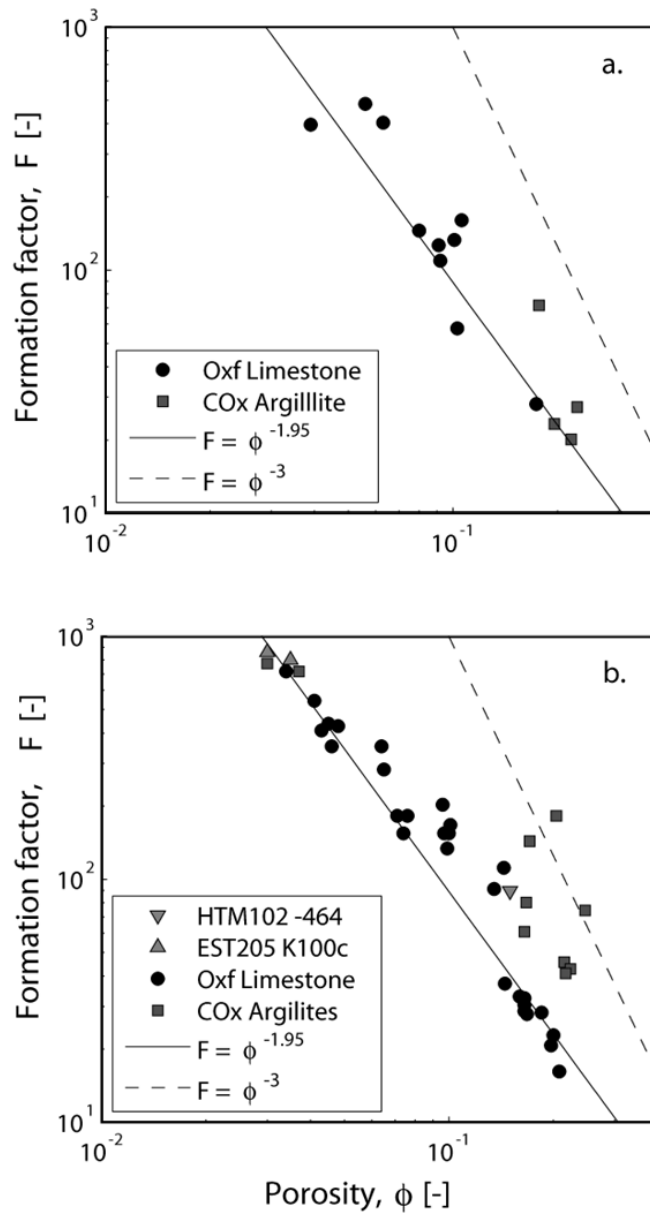


803

804

805

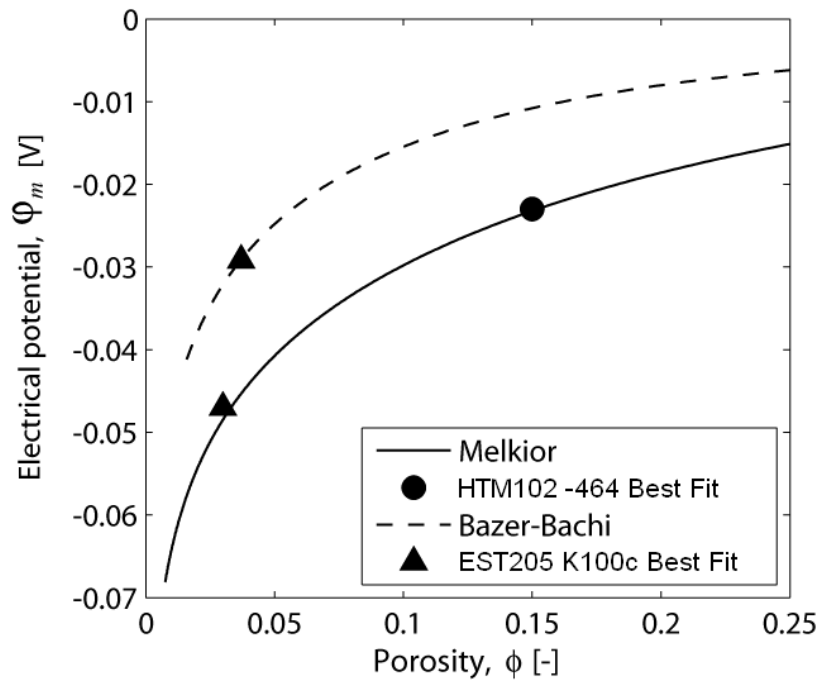
806 **Figure 7.** Formation factor versus porosity in the COx argillite. The formation factor data
 807 have been obtained: (a) by electrical measurement for Revil et al. (2005), (b) by the ratio
 808 $F = D_{HTO}^f / D_{HTO}$ for Descostes et al. (2008), and by fit for HTM102-464 and EST205-K100
 809 in the present study (a posteriori value). Archie's law for $m = 1.95$ and $m = 3$ have been
 810 proposed by Revil et al. (2005) and Descostes et al. (2008), respectively (Oxf stand for
 811 Oxfordian).



812

813

814 **Figure 8.** Fitted mean electrical potential in the three samples and model's prediction versus
 815 porosity. The mean electrical potential models are computed from the pore water chemistry
 816 used for the diffusion experiments in Melkior et al. (2007) (solid line), and in Bazer-Bachi et
 817 al. (2007) (dashed line). The data represent the best fit of experimental data of Melkior et al.
 818 (2007) and Bazer-Bachi et al. (2007) are obtained by the algorithm presented in Figure 6 on
 819 the experimental set of data (a posteriori values).

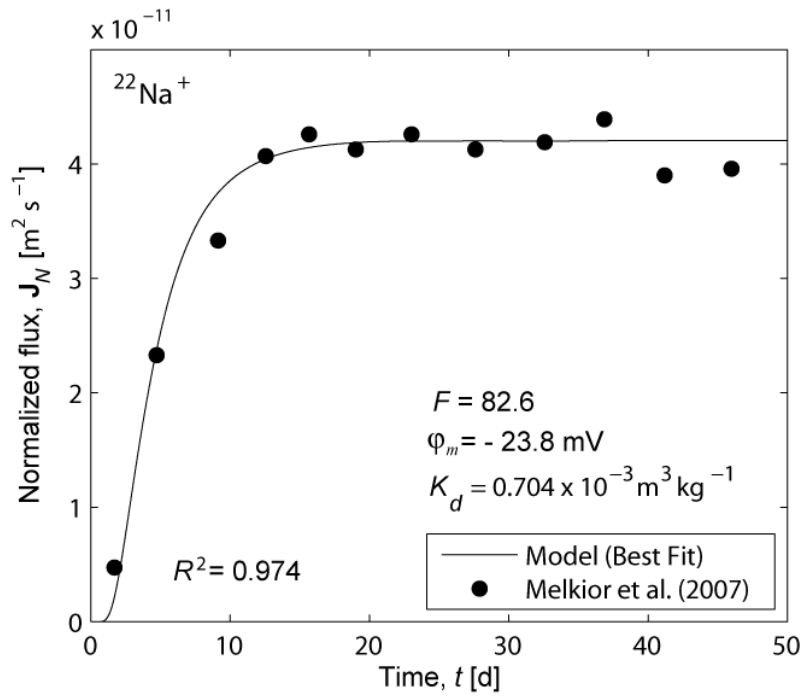


820

821

822

823 **Figure 9.** Simulation of a $^{22}\text{Na}^+$ tracer diffusion in COx (HTM102 -464m deep).
824
825



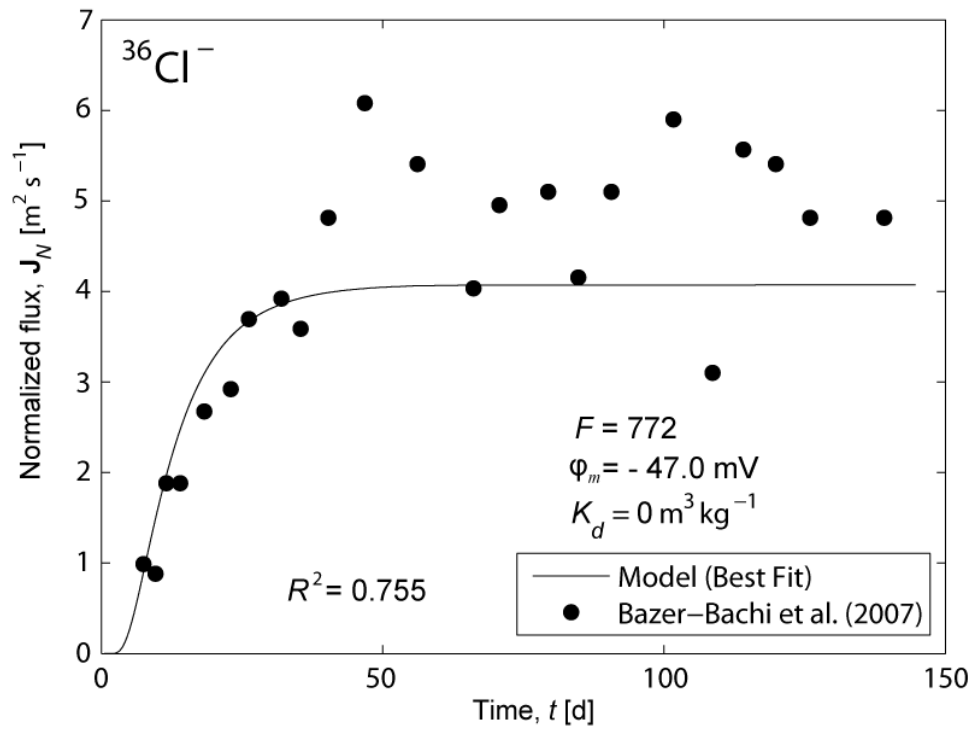
826

827

828

829 **Figure 10.** Simulation of a $^{36}\text{Cl}^-$ tracer diffusion in COx (EST205 K100).

830



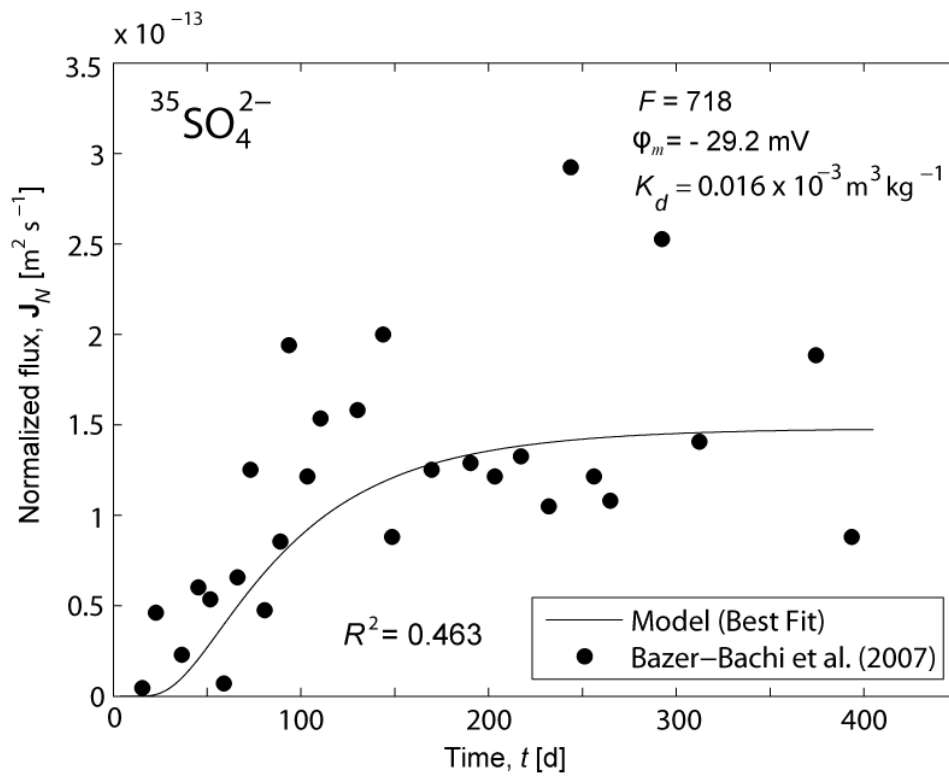
831

832

833

834 **Figure 11.** Simulation of a $^{35}\text{SO}_4^{2-}$ tracer diffusion in COx (EST205 K100).

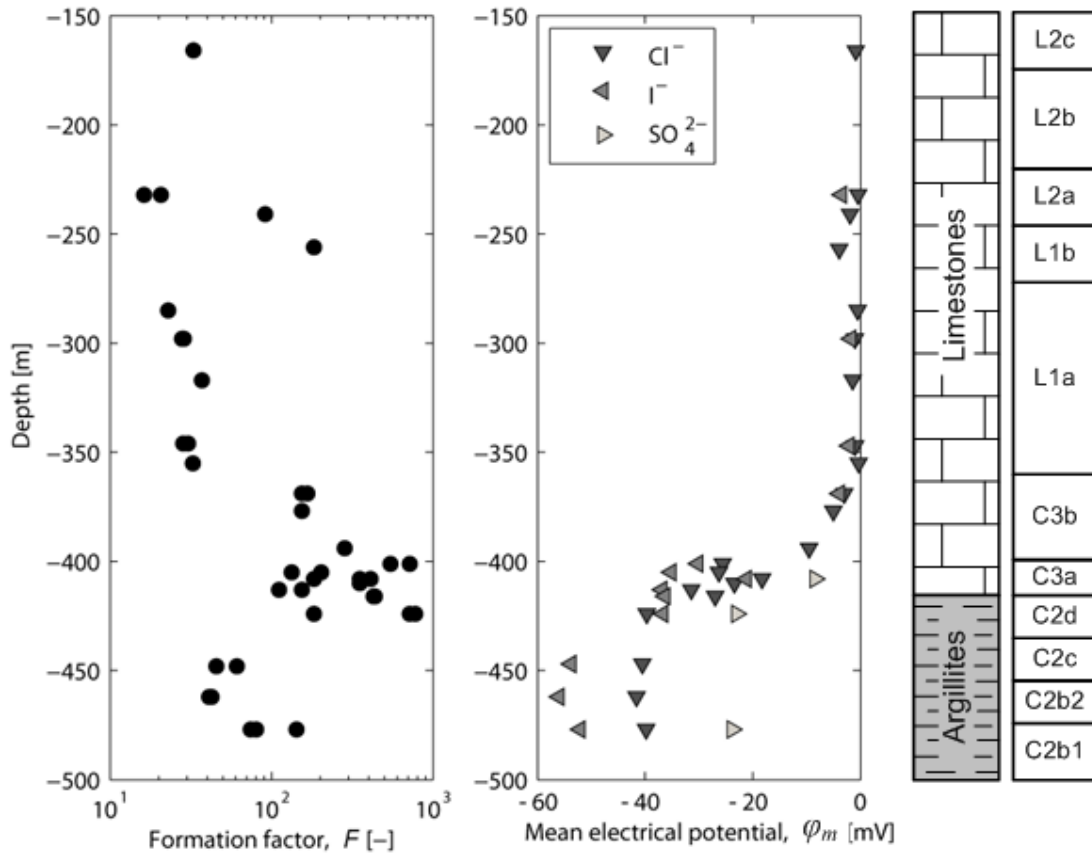
835



836

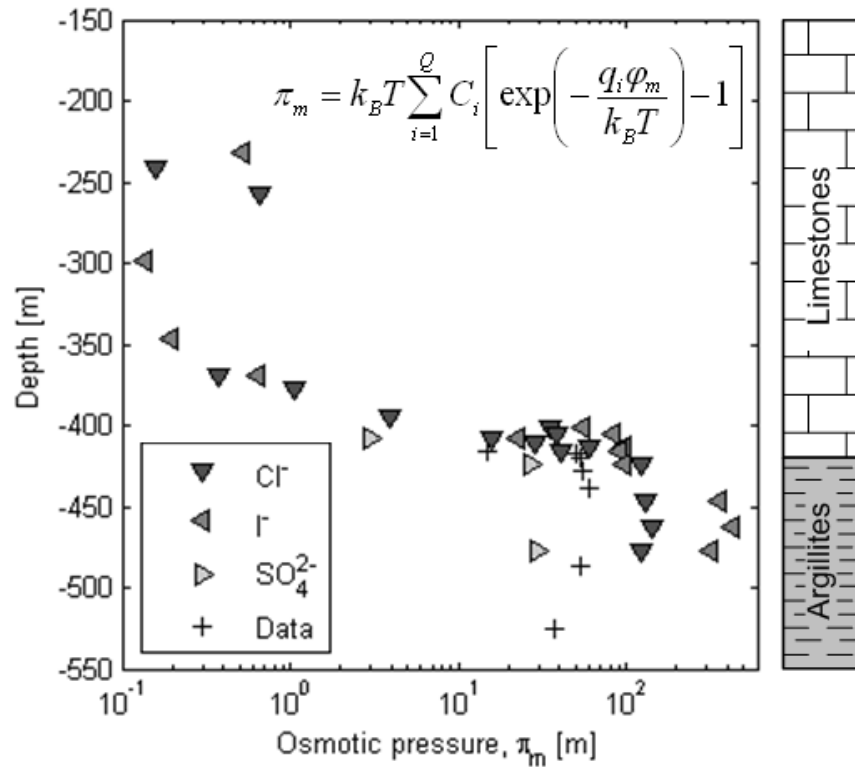
837

838 **Figure 12.** Computation of F (a) and φ_m (b) in the Bure site as a function of the depth from
 839 Descostes et al. (2008) experimental data. Samples have been collected in the well EST-205.
 840 This borehole cross the formation of Oxfordian limestones (160–417 m below ground level)
 841 and the Callovo-Oxfordian argillites (417–550 m).
 842



843
 844
 845

846 **Figure 13.** Comparison between the osmotic head π_m in the Oxfordian Limestones and
 847 Callovo-Oxfordian Argillites and the measurements of the excess pore fluid pressure head
 848 (above hydrostatic). The values of π_m have been determined from the values of φ_m (Figure 13)
 849 and synthetic pore water described in Descostes et al. (2008). The overpressure data (+) (here
 850 expressed in hydraulic head above hydrostatic) come from ANDRA (Gueutin et al., 2007).
 851



852

853